





OPEN Bifurcation, chaotic behavior, sensitivity analysis, and dynamical investigations of third-order Schrödinger equation using new auxiliary equation method

Mehreen Fatima¹, Muhammad Abbas¹, Yagoub. A. S. Arko², Tahir Nazir¹, Asnake Birhanu³ & Muhammad Zain Yousaf¹

This current study presents a precise analytical examination of the generalized third-order nonlinear Schrödinger equation through the application of the new auxiliary equation method. The approach provides several classes of exact solutions, such as V-shaped, dark soliton, periodic, kink, and anti-kink soliton solutions, which prove its effectiveness in solving higher-order nonlinear wave equations. The derived solutions are well depicted through 2D, contour, and 3D plots to show their spatial and temporal evolution features. A complete dynamical system analysis is carried out by Galilean transformation, showing the system behavior through accurate phase portraits and bifurcation diagrams. The analysis offers valuable information on stability of the solutions and transition processes amongst solution types. The system sensitivity analysis to parameters provides significant stability conditions for the solutions obtained. All the outcomes are derived by strict analytical means, and graphical plots are used to support the mathematical analysis. The study makes a contribution to the theoretical basis of nonlinear wave propagation and offers a sound framework for similar nonlinear evolution equations.

Keywords Generalized third-order nonlinear Schrödinger equation (GTNSE), New auxiliary equation method, Bifurcation analysis, Soliton solutions

The nonlinear Schrödinger equation (NLSE) is fundamental to the modeling of nonlinear wave phenomena in many different physical systems, especially in nonlinear optics, plasma physics, and fluid dynamics. Perhaps its most important application is in the description of the propagation of optical pulses in nonlinear media, for example, optical fibers, where it describes the interaction between dispersion and nonlinearity. In plasma physics¹, the NLSE controls the dynamics of wave packets in Langmuir and ion-acoustic waves. In hydrodynamics², it also models the evolution of deep-water wave trains. A distinctive feature of the NLSE is that it can support soliton solutions. Solitons are stable, localized wave structures that maintain their shape and velocity over time as a result of a fine balance between nonlinearity and dispersion. These solitons not only improved our theoretical knowledge of nonlinear systems but also resulted in practical applications, like distortion-free long-distance communication using fiber-optic cables.

Based on the fundamental applications of NLSE, it is extended by adding higher effects like third-order dispersion, self-steepening, and stimulated Raman scattering. The most significant advancement is the generalized third-order nonlinear Schrödinger equation (GTNSE)³. The higher effects are required in the transmission of ultrashort optical pulses in high-speed communications or in complex nonlinear materials with complicated dispersion. The GTNSE offers a more precise model for describing complex wave dynamics in nonlinear optics, plasma waves, and fluid dynamics where second-order models are inadequate. Similar to the NLSE, the GTNSE also possesses soliton solutions, which can take more complicated forms like dark, bright, kink-type, and rogue solitons based on how the higher-order terms interact. The soliton solutions of the GTNSE

¹Department of Mathematics, University of Sargodha, Sargodha 40100, Pakistan. ²Department of Mathematics, Turabah University College, Taif University, P.O. Box 11099, 21944 Taif, Saudi Arabia. ³Department of Mathematics, College of Science, Hawassa University, Hawassa, Ethiopia. ✉email: muhammad.abbas@uos.edu.pk; asnakeb@hu.edu.et

are crucial in understanding advanced phenomena like pulse compression, and stability of localized wave packets in nonlinear and dispersive materials. Due to its relevance in modeling real phenomena, a broad range of analytical and numerical methods has been developed to study its solutions.

Development of new analytical methods in recent years has significantly improved our capacity for finding the exact solutions of such nonlinear evolution equations. Some of them are modified, the first-integral method⁴, the $(\frac{G'}{G})$ -expansion method⁵, the improved $(\frac{G'}{G})$ -expansion method⁶, Sine-cosine method⁷ and the sub-ODE method⁸. In addition, the Hirota bilinear method^{9,10}, Modified kudryashov expansion method¹¹, rational sine and rational cosine methods^{12,13}, Kudryashov expansion¹⁴, extended tanh(coth)-expansion method¹⁵ and updated rational sine-cosine-function method have gained attention¹⁶. Overall, these methods highlights the importance of analytical method in soliton dynamics. Sardar sub equation method¹⁷ and new extended and modified rational expansion method¹⁸ have been used to successfully solve the GTNSE and derive various types of solutions ranging from bright, dark, and singular solitons to periodic and chaotic waveforms. Ahmad, et al.¹⁹ investigate the fractional GTNSE by using generalized riccati equation and mapping method. Badshah, et al.²⁰ explore the soliton solutions by using improved F-expansion method, extended hyperbolic function technique and Adomian decomposition method and applied modulation stability to verify the results.

The primary objective of this research is to obtain traveling wave solutions of the GTNSE by an effective and rigorous technique known as the new auxiliary equation method (NAEM). The technique enables us to simplify the original PDE to an easier ODE by appropriate transformations and the introduction of auxiliary functions, enabling us to obtain explicit analytical solutions. Using the technique, we obtain several exact solutions, including soliton, periodic, and rational-type waveforms, demonstrating the intricate math structure of the model behind. In addition to discovering exact solutions, we perform a careful analysis of the traveling wave system. Bifurcation analysis shows how system parameters affect the model's performance and the shape of the solutions. Specifically, we investigate dynamics of the reduced ODE system, identify the transitions between the many dynamical states and determine equilibrium points, phase portrait and inspect conditions under which saddle-node, center, or spiral-type bifurcations occur, which improves our comprehension of the solutions' structural characteristics. This work integrates the new auxiliary equation method and bifurcation analysis to further investigate the intricate behavior modelled by the GTNSE. Our study generates new exact solutions and offers informative analytical explanations for the broader area of nonlinear wave theory.

The paper is organized into sections. Governing equation is describe in Sect. 2. Section 3 covered algorithm of new auxiliary method in detail. In Sect. 4, method is implemented. Visual evaluation and discussion is explained in Sect. 5. Bifurcation analysis is done in Sect. 6. Chaotic behaviour and sensitivity analysis is examined in Sects. 7 and 8, respectively. Physical significance of study is describe in Sect. 9. Then conclusion is provided.

Governing equation

The GTNSE is a mathematical model, an extension of the original nonlinear Schrödinger equation, which is applied to model wave propagation in nonlinear media. The GTNSE²¹ is:

$$i(u_t + u_{xxx}) + |u|^2(\beta_1 u + i\beta_2 u_x) + i\beta_3(|u|^2)_x u = 0, \quad (2.1)$$

where the dispersive coefficient is indicated by parameters β_2 and β_3 , the coefficient of cubic nonlinearity is represented by parameter β_1 and $u = u(x, t)$ is a complex function. Eq. (2.1) has been used to model ultrashort pulses in optical fibers. The above equation typically also contains the term of second-order derivative. But as soon as the derivative expression of third order is added, the second-order derivative term can be eliminated through a gauge transformation formation. If $\beta_1 = \beta_3 = 0$, then Eq. (2.1) is termed as modified Korteweg-de Vries or Hirota equation in complex form, which can be solved by the inverse scattering transform technique.

Algorithm of new auxiliary equation method

The procedures for using the auxiliary equation approach²² to find traveling wave solutions of nonlinear partial differential equations are described in this section.

Consider the general form of nonlinear partial differential equations (NLPDE), involving two independent variables x and t , expressed as follows:

$$P_1(u, u_t, u_x, u_{tt}, u_{xx}, u_{xxx}, \dots) = 0, \quad (3.1)$$

where function $u = u(x, t)$ is complex function. P_1 is the polynomial expression involving functions and their classical derivatives, where the maximum order of derivative and nonlinear terms are co-related. Detailed and concise flowchart of solutions procedure is given in Fig. 1.

Step 1: Apply the wave transformation, given as follow:

$$u(x, t) = \Psi(\xi) e^{i\phi}, \quad \text{where } \xi = x - \gamma t, \quad \phi = \omega t - \eta x + \delta. \quad (3.2)$$

Here γ, ω, η represents soliton's velocity, wave number and frequency, respectively. Phase constant is denoted by δ .

Step 2: The transformation in step 1, converts NLPDE in Eq. (3.1) to nonlinear ordinary differential equation :

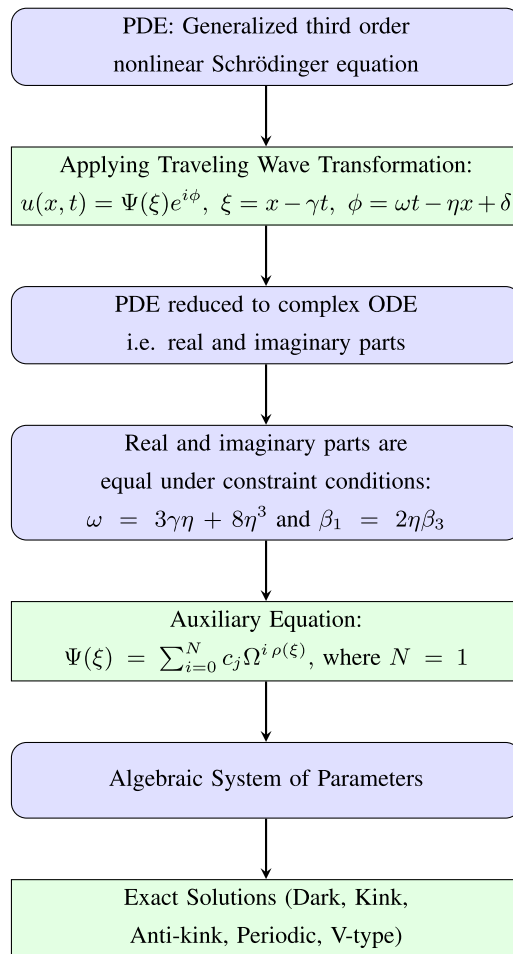


Fig. 1. Solution procedure for GTNSE via NAEM.

$$P_1 (\Psi, \Psi', \Psi'', \Psi''', \dots) = 0, \tag{3.3}$$

Step 3: Now according to NAEM, the Eq. (3.3) has series solution of the form:

$$\Psi(\xi) = \sum_{i=0}^N c_j \Omega^{i \rho(\xi)}, \tag{3.4}$$

where $c_j (j = 0, 1, 2, \dots, N)$ are constants. $\rho(\xi)$ satisfies the following equation:

$$\rho'(\xi) = \frac{1}{\ln \Omega} (\zeta \Omega^{-\rho(\xi)} + \chi + \theta \Omega^{\rho(\xi)}), \quad \Omega > 0, \Omega \neq 1 \tag{3.5}$$

where ζ, θ and χ are real constant parameters. Depending on these constants, specific solutions of (3.5) are determined.

Step 4 The positive integer N is obtained by balancing highest-order derivative with the highest-degree non-linear term in Eq. (3.3).

Step 5 Then, put Eq. (3.4) along with Eq. (3.5) in Eq. (3.3). An algebraic system is obtained by setting all like-terms of $\Omega^{\rho(\xi)}$ equal to zero. Solve the obtained system to find the values of unknown parameters. Then, put these parameters into Eq. (3.4) along with solutions of $\Omega^{\rho(\xi)}$ stated below : Following families are produced using general solution with $\Gamma = (\chi^2 - 4\zeta\theta)$:

Cluster 1: When $\theta \neq 0$, and $\Gamma = (\chi^2 - 4\zeta\theta) < 0$, then

$$\Omega^{\rho(\xi)} = -\frac{\chi}{2\theta} + \frac{\sqrt{-\Gamma}}{2\theta} \tan\left(\frac{\sqrt{-\Gamma}}{2}\xi\right),$$

$$\Omega^{\rho(\xi)} = -\frac{\chi}{2\theta} - \frac{\sqrt{-\Gamma}}{2\theta} \cot\left(\frac{\sqrt{-\Gamma}}{2}\xi\right).$$

Cluster 2: When $\theta \neq 0$, and $\Gamma = (\chi^2 - 4\zeta\theta) > 0$, then

$$\Omega^{\rho(\xi)} = -\frac{\chi}{2\theta} - \frac{\sqrt{\Gamma}}{2\theta} \tanh\left(\frac{\sqrt{\Gamma}}{2}\xi\right),$$

$$\Omega^{\rho(\xi)} = -\frac{\chi}{2\theta} - \frac{\sqrt{\Gamma}}{2\theta} \coth\left(\frac{\sqrt{\Gamma}}{2}\xi\right).$$

Cluster 3: When $4\zeta^2 + \chi^2 < 0$, $\theta = -\zeta$ and $\theta \neq 0$, then

$$\Omega^{\rho(\xi)} = \frac{\chi}{2\zeta} - \frac{\sqrt{-(\chi^2 + 4\zeta^2)}}{2\zeta} \tan\left(\frac{\sqrt{-(\chi^2 + 4\zeta^2)}}{2}\xi\right),$$

$$\Omega^{\rho(\xi)} = \frac{\chi}{2\zeta} + \frac{\sqrt{-(\chi^2 + 4\zeta^2)}}{2\zeta} \cot\left(\frac{\sqrt{-(\chi^2 + 4\zeta^2)}}{2}\xi\right).$$

Cluster 4: When $4\zeta^2 + \chi^2 > 0$, $\theta = -\zeta$ and $\theta \neq 0$, then

$$\Omega^{\rho(\xi)} = \frac{\chi}{2\zeta} + \frac{\sqrt{(\chi^2 + 4\zeta^2)}}{2\zeta} \tanh\left(\frac{\sqrt{(\chi^2 + 4\zeta^2)}}{2}\xi\right),$$

$$\Omega^{\rho(\xi)} = \frac{\chi}{2\zeta} + \frac{\sqrt{(\chi^2 + 4\zeta^2)}}{2\zeta} \coth\left(\frac{\sqrt{(\chi^2 + 4\zeta^2)}}{2}\xi\right).$$

Cluster 5: When $\chi^2 - 4\zeta^2 < 0$ and $\theta = \zeta$, then

$$\Omega^{\rho(\xi)} = -\frac{\chi}{2\zeta} + \frac{\sqrt{-(\chi^2 - 4\zeta^2)}}{2\zeta} \tan\left(\frac{\sqrt{-(\chi^2 - 4\zeta^2)}}{2}\xi\right),$$

$$\Omega^{\rho(\xi)} = -\frac{\chi}{2\zeta} - \frac{\sqrt{-(\chi^2 - 4\zeta^2)}}{2\zeta} \cot\left(\frac{\sqrt{-(\chi^2 - 4\zeta^2)}}{2}\xi\right).$$

Cluster 6: When $\chi^2 - 4\zeta^2 > 0$ and $\theta = \zeta$, then

$$\Omega^{\rho(\xi)} = -\frac{\chi}{2\zeta} - \frac{\sqrt{(\chi^2 - 4\zeta^2)}}{2\zeta} \tanh\left(\frac{\sqrt{(\chi^2 - 4\zeta^2)}}{2}\xi\right),$$

$$\Omega^{\rho(\xi)} = -\frac{\chi}{2\zeta} - \frac{\sqrt{(\chi^2 - 4\zeta^2)}}{2\zeta} \coth\left(\frac{\sqrt{(\chi^2 - 4\zeta^2)}}{2}\xi\right).$$

Cluster 7: When $\chi^2 = 4\theta\zeta$, then

$$\Omega^{\rho(\xi)} = -\frac{2 + \chi\xi}{2\theta\xi}.$$

Cluster 8: When $\zeta\theta < 0$, $\theta \neq 0$ and $\chi = 0$, then

$$\Omega^{\rho(\xi)} = -\sqrt{\frac{-\zeta}{\theta}} \tanh\left(\sqrt{-\zeta\theta}\xi\right),$$

$$\Omega^{\rho(\xi)} = -\sqrt{\frac{-\zeta}{\theta}} \coth\left(\sqrt{-\zeta\theta}\xi\right).$$

Cluster 9: When $\zeta = -\theta$ and $\chi = 0$, then

$$\Omega^{\rho(\xi)} = -\left(\frac{1 + e^{-2\theta\xi}}{1 - e^{-2\theta\xi}}\right).$$

Cluster 10: When $\zeta = \theta = 0$, then

$$\Omega^{\rho(\xi)} = \sinh(\chi\xi) - \cosh(\chi\xi).$$

Cluster 11: When $\zeta = L = \chi$ and $\theta = 0$, then

$$\Omega^{\rho(\xi)} = e^{L\xi} - 1.$$

Cluster 12: If $\theta = L = \chi$ and $\zeta = 0$, then

$$\Omega^{\rho(\xi)} = \frac{e^{L\xi}}{1 - e^{L\xi}}.$$

Cluster 13: If $\chi = \zeta + \theta$, then

$$\Omega^{\rho(\xi)} = -\frac{1 - \zeta e^{(\zeta - \theta)\xi}}{1 - \theta e^{(\zeta - \theta)\xi}}.$$

Cluster 14: When $\chi = -\zeta - \theta$, then

$$\Omega^{\rho(\xi)} = \frac{e^{(\zeta - \theta)\xi} - \zeta}{e^{(\zeta - \theta)\xi} - \theta}.$$

Cluster 15: When $\zeta = 0$, then

$$\Omega^{\rho(\xi)} = \frac{\chi e^{\chi\xi}}{1 - \theta e^{\chi\xi}}.$$

Cluster 16: When $\zeta = \chi = \theta \neq 0$, then

$$\Omega^{\rho(\xi)} = \frac{1}{2} \left(\sqrt{3} \tan \left(\frac{\sqrt{3}}{2} \zeta \xi \right) - 1 \right).$$

Cluster 17: When $\chi = \theta = 0$, then

$$\Omega^{\rho(\xi)} = \zeta \xi.$$

Cluster 18: When $\zeta = \chi = 0$, then

$$\Omega^{\rho(\xi)} = \frac{-1}{\theta \xi}.$$

Cluster 19: When $\zeta = \theta$ and $\chi = 0$, then

$$\Omega^{\rho(\xi)} = \tan(\zeta \xi).$$

Cluster 20: When $\theta = 0$, then

$$\Omega^{\rho(\xi)} = e^{\chi\xi} - \frac{n}{l}.$$

Applications

Travelling wave transformation for GTNSE

Substitute transformation provided in Eqs. (3.2) to (2.1), then separate real part (Re) and imaginary part (Im) of resulting equation.

$$\begin{cases} Re : -\eta^3 \Psi - \omega \Psi + \beta_1 \Psi^3 + \eta \beta_2 \Psi^3 + 3\eta \Psi'' = 0, \\ Im : -\gamma \Psi' - 3\eta^2 \Psi' + \beta_2 \Psi^2 \Psi + 2\beta_3 \Psi^2 \Psi + \Psi''' = 0. \end{cases} \quad (4.1)$$

Now, by integrating imaginary part and setting constant of integration to zero, yields:

$$-\gamma \Psi - 3\eta^2 \Psi + \frac{1}{3} \beta_2 \Psi^3 + \frac{2}{3} \beta_3 \Psi^3 + \Psi'' = 0. \quad (4.2)$$

The Eq. (4.1) and Eq. (4.2) are equal under following constraints:

$$\omega = 3\gamma \eta + 8\eta^3, \quad \beta_1 = 2\eta \beta_3.$$

Plug these constraints into Eq. (4.1), yields

$$(-3\gamma\eta - 9\eta^3)\Psi + (\beta_2\eta + 2\beta_3\eta)\Psi^3 + 3\eta\Psi'' = 0. \quad (4.3)$$

Application of new auxiliary equation method

Using balancing principle that equate the highest order derivative with the highest degree nonlinear term in Eq. (4.3), results in $N = 1$. Now, with help of Eq. (3.4), series solution of Eq. (4.3) becomes:

$$\Psi(\xi) = c_0 + c_1 \Omega^{\rho(\xi)}. \quad (4.4)$$

A nonlinear system in $\Omega^{\rho(\xi)}$ is obtained by substituting the above solution along with Eq. (3.5) into Eq. (4.3). Now, arrange all terms in power of $\Omega^{\rho(\xi)}$. An algebraic system is obtained by setting each coefficients of generated polynomial equal to zero, that is

$$\begin{cases} (\Omega^{\rho(\xi)})^0 = -3\gamma\eta c_0 - 9\eta^3 c_0 + 3\zeta\eta\chi c_1 + \eta c_0^3 \beta_2 + 2\eta c_0^3 \beta_3, \\ (\Omega^{\rho(\xi)})^1 = -3\gamma\eta c_1 - 9\eta^3 c_1 + 6\zeta\eta\theta c_1 + 3\eta\chi^2 c_1 + 3\eta c_0^2 c_1 \beta_2 + 6\eta c_0^2 c_1 \beta_3, \\ (\Omega^{\rho(\xi)})^2 = 9\eta\theta\chi c_1 + 3\eta c_0 c_1^2 \beta_2 + 6\eta c_0 c_1^2 \beta_3, \\ (\Omega^{\rho(\xi)})^3 = 6\eta\theta^2 c_1 + \eta c_1^3 \beta_2 + 2\eta c_1^3 \beta_3. \end{cases}$$

Then, solve this system by using software Wolfram Mathematica, the following parameters are obtained:

$$c_1 = \frac{2\theta c_0}{\chi}, \gamma = \frac{1}{2}(-6\eta^2 + 4\zeta\theta - \chi^2), \beta_3 = \frac{-3\chi^2 - 2c_0^2 \beta_2}{4c_0^2}.$$

Using the families of solutions described in section 3, the analytical solutions of GTNSE are presented as follows:

Cluster 1: When $\theta \neq 0$, and $\Gamma = (\chi^2 - 4\zeta\theta) < 0$, then

$$\begin{aligned} \Omega^{\rho(\xi)} &= \frac{e^{i\phi} \sqrt{-\Gamma} c_0 \tan\left(\frac{\sqrt{-\Gamma}}{2} \xi\right)}{\chi}, \\ \Omega^{\rho(\xi)} &= -\frac{e^{i\phi} \sqrt{-\Gamma} c_0 \cot\left(\frac{\sqrt{-\Gamma}}{2} \xi\right)}{\chi}. \end{aligned}$$

Cluster 2: When $\theta \neq 0$, and $\Gamma = (\chi^2 - 4\zeta\theta) > 0$, then

$$\begin{aligned} \Omega^{\rho(\xi)} &= -\frac{e^{i\phi} \sqrt{\Gamma} c_0 \tanh\left(\frac{\sqrt{\Gamma}}{2} \xi\right)}{\chi}, \\ \Omega^{\rho(\xi)} &= -\frac{e^{i\phi} \sqrt{\Gamma} c_0 \coth\left(\frac{\sqrt{\Gamma}}{2} \xi\right)}{\chi}. \end{aligned} \quad (4.5)$$

Cluster 3: When $4\zeta^2 + \chi^2 < 0$, $\theta = -\zeta$ and $\theta \neq 0$, then

$$\begin{aligned} \Omega^{\rho(\xi)} &= \frac{1}{\zeta\chi} e^{i\phi} c_0 \left((\zeta + \theta)\chi - \theta \sqrt{-(4\zeta^2 + \chi^2)} \tan\left(\frac{\sqrt{-(4\zeta^2 + \chi^2)}}{2} \xi\right) \right), \\ \Omega^{\rho(\xi)} &= \frac{1}{\zeta\chi} e^{i\phi} c_0 \left((\zeta + \theta)\chi + \theta \sqrt{-(4\zeta^2 + \chi^2)} \cot\left(\frac{\sqrt{-(4\zeta^2 + \chi^2)}}{2} \xi\right) \right). \end{aligned}$$

Cluster 4: When $4\zeta^2 + \chi^2 > 0$, $\theta = -\zeta$ and $\theta \neq 0$, then

$$\Omega^{\rho(\xi)} = \frac{1}{\zeta\chi} e^{i\phi} c_0 \left((\zeta + \theta)\chi + \theta \sqrt{4\zeta^2 + \chi^2} \tanh\left(\frac{\sqrt{4\zeta^2 + \chi^2}}{2} \xi\right) \right), \quad (4.6)$$

$$\Omega^{\rho(\xi)} = \frac{1}{\zeta\chi} e^{i\phi} c_0 \left((\zeta + \theta)\chi + \theta \sqrt{4\zeta^2 + \chi^2} \coth\left(\frac{\sqrt{4\zeta^2 + \chi^2}}{2} \xi\right) \right). \quad (4.7)$$

Cluster 5: When $\chi^2 - 4\zeta^2 < 0$ and $\theta = \zeta$, then

$$\begin{aligned}\Omega^{\rho(\xi)} &= \frac{1}{\zeta\chi} e^{i\phi} c_0 \left((\zeta - \theta)\chi + \theta\sqrt{4\zeta^2 - \chi^2} \tan\left(\frac{\sqrt{4\zeta^2 - \chi^2}}{2}\xi\right) \right), \\ \Omega^{\rho(\xi)} &= \frac{1}{\zeta\chi} e^{i\phi} c_0 \left((\zeta - \theta)\chi - \theta\sqrt{4\zeta^2 - \chi^2} \cot\left(\frac{\sqrt{4\zeta^2 - \chi^2}}{2}\xi\right) \right).\end{aligned}\quad (4.8)$$

Cluster 6: When $\chi^2 - 4\zeta^2 > 0$ and $\theta = \zeta$, then

$$\begin{aligned}\Omega^{\rho(\xi)} &= \frac{1}{\zeta\chi} e^{i\phi} c_0 \left((\zeta - \theta)\chi - \theta\sqrt{\chi^2 - 4\zeta^2} \tanh\left(\frac{\sqrt{\chi^2 - 4\zeta^2}}{2}\xi\right) \right), \\ \Omega^{\rho(\xi)} &= \frac{1}{\zeta\chi} e^{i\phi} c_0 \left((\zeta - \theta)\chi - \theta\sqrt{\chi^2 - 4\zeta^2} \coth\left(\frac{\sqrt{\chi^2 - 4\zeta^2}}{2}\xi\right) \right).\end{aligned}\quad (4.9)$$

Cluster 7: When $\chi^2 = 4\theta\zeta$, then

$$\Omega^{\rho(\xi)} = -\frac{2e^{i\phi} c_0}{\xi\chi}.$$

Cluster 8: When $\zeta\theta < 0$, $\theta \neq 0$ and $\chi = 0$, then

$$\begin{aligned}\Omega^{\rho(\xi)} &= \frac{e^{i\phi} c_0 \left(\chi - 2\sqrt{-\frac{\zeta}{\theta}} \theta \tanh(\sqrt{-\zeta\theta}\xi) \right)}{\chi}, \\ \Omega^{\rho(\xi)} &= \frac{e^{i\phi} c_0 \left(\chi - 2\sqrt{-\frac{\zeta}{\theta}} \theta \coth(\sqrt{-\zeta\theta}\xi) \right)}{\chi}.\end{aligned}$$

Cluster 9: When $\zeta = -\theta$ and $\chi = 0$, then

$$\Omega^{\rho(\xi)} = e^{i\phi} \left(1 - \frac{2(1 + e^{2\theta\xi})\theta}{(-1 + e^{2\theta\xi})\chi} \right) c_0.$$

Cluster 10: When $\zeta = \theta = 0$, then

$$\Omega^{\rho(\xi)} = \frac{1}{\chi} e^{i\phi} (\chi - 2\theta \cosh(\xi\chi) + 2\theta \sinh(\xi\chi)) c_0.$$

Cluster 11: When $\zeta = K = \chi$ along with $\theta = 0$, then

$$\Omega^{\rho(\xi)} = \frac{e^{i\phi} (2(-1 + e^{K\xi})\theta + \chi) c_0}{\chi}.$$

Cluster 12: When $\theta = K = \chi$ and $\zeta = 0$, then

$$\Omega^{\rho(\xi)} = e^{i\phi} \left(1 + \frac{2e^{K\xi}\theta}{\chi - e^{K\xi}\chi} \right) c_0.$$

Cluster 13: When $\chi = \zeta + \theta$, then

$$\Omega^{\rho(\xi)} = e^{i\phi} \left(1 + \frac{2 \left(-\zeta + \frac{-\zeta + \theta}{-1 + e^{(\zeta - \theta)\xi}} \right)}{\chi} \right) c_0.$$

Cluster 14: When $\chi = -\zeta - \theta$, then

$$\Omega^{\rho(\xi)} = e^{i\phi} \left(1 + \frac{2(e^{(\zeta-\theta)\xi} - \zeta)\theta}{(e^{(\zeta-\theta)\xi} - \theta)\chi} \right) c_0.$$

Cluster 15: When $\zeta = 0$, then

$$\Omega^{\rho(\xi)} = -\frac{e^{i\phi} (1 + \theta e^{\xi\chi}) c_0}{-1 + \theta e^{\xi\chi}}.$$

Cluster 16: When $\zeta = \chi = \theta \neq 0$, then

$$\Omega^{\rho(\xi)} = \frac{e^{i\phi} c_0 \left(\chi + \sqrt{3}\theta \tan\left(\frac{\sqrt{3}}{2}\zeta\xi\right) \right)}{\chi}.$$

Cluster 17: When $\chi = \theta = 0$, then

$$\Omega^{\rho(\xi)} = \frac{e^{i\phi} (2\zeta\theta\xi + \chi) c_0}{\chi}.$$

Cluster 18: When $\zeta = \chi = 0$, then

$$\Omega^{\rho(\xi)} = \frac{e^{i\phi} (-2 + \xi\chi) \cdot c_0}{\xi\chi}.$$

Cluster 19: When $\zeta = \theta$ and $\chi = 0$, then

$$\Omega^{\rho(\xi)} = \frac{e^{i\phi} c_0 (\chi + 2\theta \tan(\zeta\xi))}{\chi}.$$

Cluster 20: When $\theta = 0$, then

$$\Omega^{\rho(\xi)} = e^{i\phi} \left(1 + \frac{2(e^{\xi\chi} - \frac{n}{l})\theta}{\chi} \right) c_0.$$

where $\xi = x - \gamma t$, and $\phi = \omega t - \eta x + \delta$.

Limiting cases and comparison

In addition to broadening the scope of current analytical techniques, the analytical solutions of the GTNSE obtained using the NAEM also recover a number of classical solutions when the parameters are limited to certain values. By choosing properly the auxiliary parameters ζ , χ , θ and Ω in the equation,

$$\rho'(\xi) = \frac{1}{\ln \Omega} (\zeta \Omega^{-\rho(\xi)} + \chi + \theta \Omega^{\rho(\xi)}), \quad \Omega > 0, \Omega \neq 1,$$

the general solution $\Psi(\xi) = c_0 + c_1 \Omega^{\rho(\xi)}$ simplifies to classical waves forms and solitons described in literature. Specifically, when $\theta = -\zeta$, $\chi = 0$, and $\Omega = e$, the solution leads to $\Omega^{\rho(\xi)} = -\tanh(\xi)$ or $-\coth(\xi)$, corresponding to kink and dark solitons. These are same as standard solutions for GTNSE derived by using tanh-coth method²³. Similarly, when $\chi^2 - 4\zeta\theta < 0$, trigonometric solutions such as $\tan(-\Gamma\xi)$ or $\cot(-\Gamma\xi)$ arise, corresponding with periodic wave solutions obtained by the modified $(\frac{\zeta'}{G})$ -expansion approach^{24,25}. In the case $\chi^2 = 4\zeta\theta$, rational solutions of the form $\Omega^{\rho(\xi)} = -\frac{-2+\chi\xi}{2\theta\xi}$ are derived, which represent algebraic or rogue wave-type solutions^{26,27}. Moreover, the NAEM framework consolidates other current methodologies. As a result, the NAEM proves itself effective in generating a range of accurate solutions in addition to acting as a unified framework incorporating a wide range of standard approaches as definitive examples. Such consistency with standard results thus verifies the method's potency and reliance in solving nonlinear evolution equations, thus raising its theoretical significance in the broader application area of soliton theory.

Visual evaluations and discussion

This section presents a detailed analysis of the traveling wave solutions derived by using the NAEM for GTNSE. This equation has extensive application in the modeling of nonlinear complex wave processes in nonlinear optics, plasma physics, hydrodynamics, and ultra-short pulse propagation. With the implementation of the novel method, a richness of exact wave solutions have been obtained successfully, such as dark solitons, V-type solitons, periodic waves, kink, and anti-kink wave profiles. This diversity of profiles indicates the success and effectiveness of the proposed method in generating physically meaningful solutions. In contrast to earlier published results, the findings here prove higher diversity and accuracy in the solutions achieved. The invariance and stability of

such solutions under propagation attest to their usability within the modeling of actual nonlinear systems. To further clarify the dynamical behavior and space evolution of the solutions derived, graphical illustrations are presented in 2D, 3D, and contour plots. Contour plots specifically assist in the description of the wave intensity distribution and topological structure in various spatial regions.

The results of applying NAEM is discussed below:

- Dark soliton represented in Fig. 2, obtained from Eq. (4.5), create stable intensity dip with jumps in phase when nonlinearity compensates normal dispersion. These solutions have good propagation properties and can be used in optical switching applications and dark pulse generation.
- Figure 3 illustrate anti-kink soliton solution provided in Eq. (4.6), with inverted phase profiles in contrast to kink solitons.
- Figure 4 illustrate periodic solution, obtained from Eq. (4.7), demonstrate stable intensity modulation. Such solutions are useful for designing all-optical buffers and waveguide arrays.
- V-shaped soliton as shown in Fig. 5, is found in Eq. (4.8) which are defined by their vertex-like intensity profiles with conjugate phase jumps. These solutions have uses in optical pulse compression and frequency comb generation.
- Kink solitons in Fig. 6 arise in Eq. (4.9), with monotonic phase transitions between stable solutions. Such topological solitons are used to make optical logic gates.

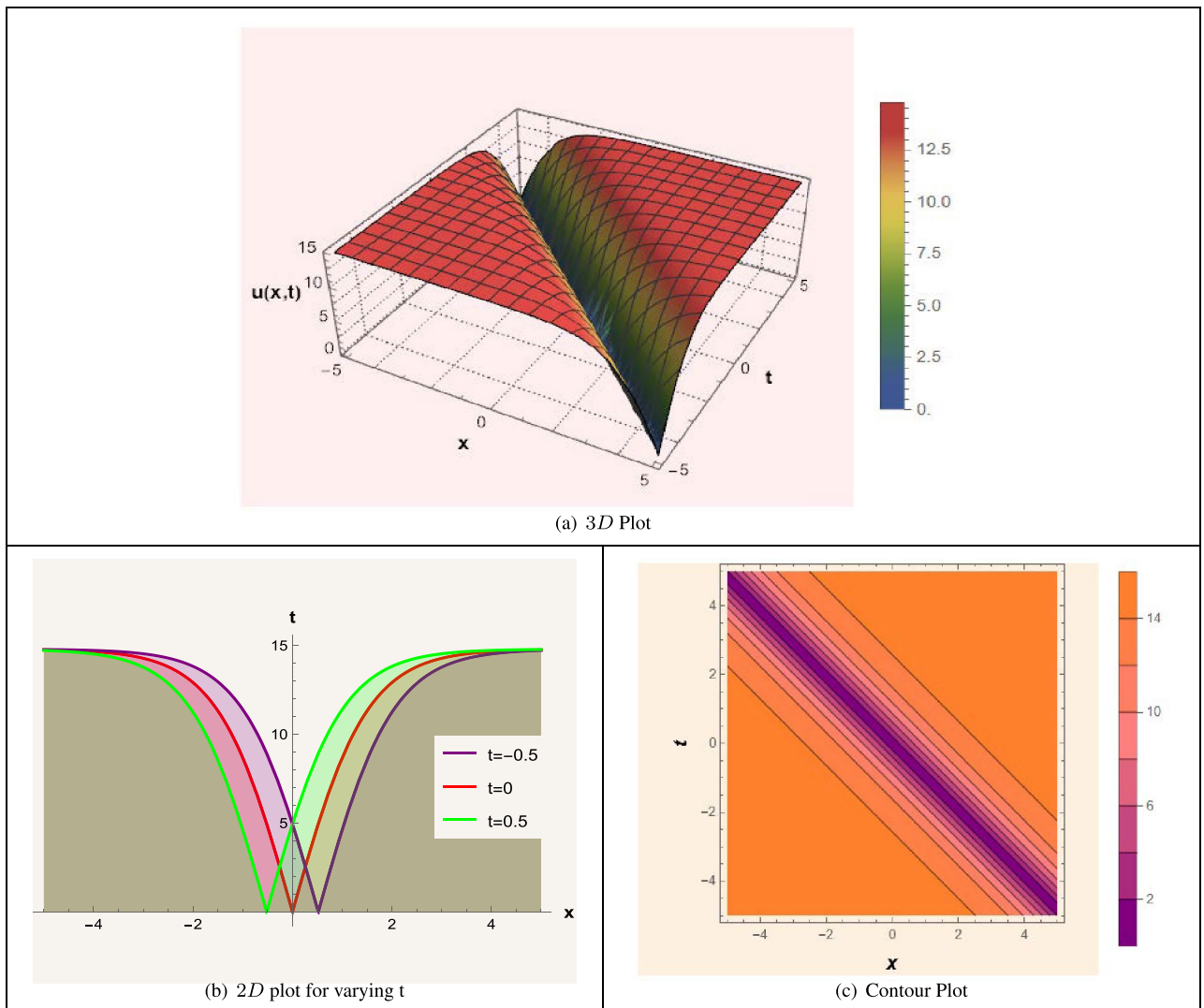


Fig. 2. Dark soliton solution of absolute behaviour for Eq. (4.5) by employing the parametric values: (a) 3D plot illustrates the intensity dip's progression along the x - t plane; (b) 2D profile demonstrate the dip's propagation at $t = 0$ (red line), $t = -0.5$ (purple line) and $t = 0.5$ (green line); (c) a contour plot shows the phase jump over the soliton core.

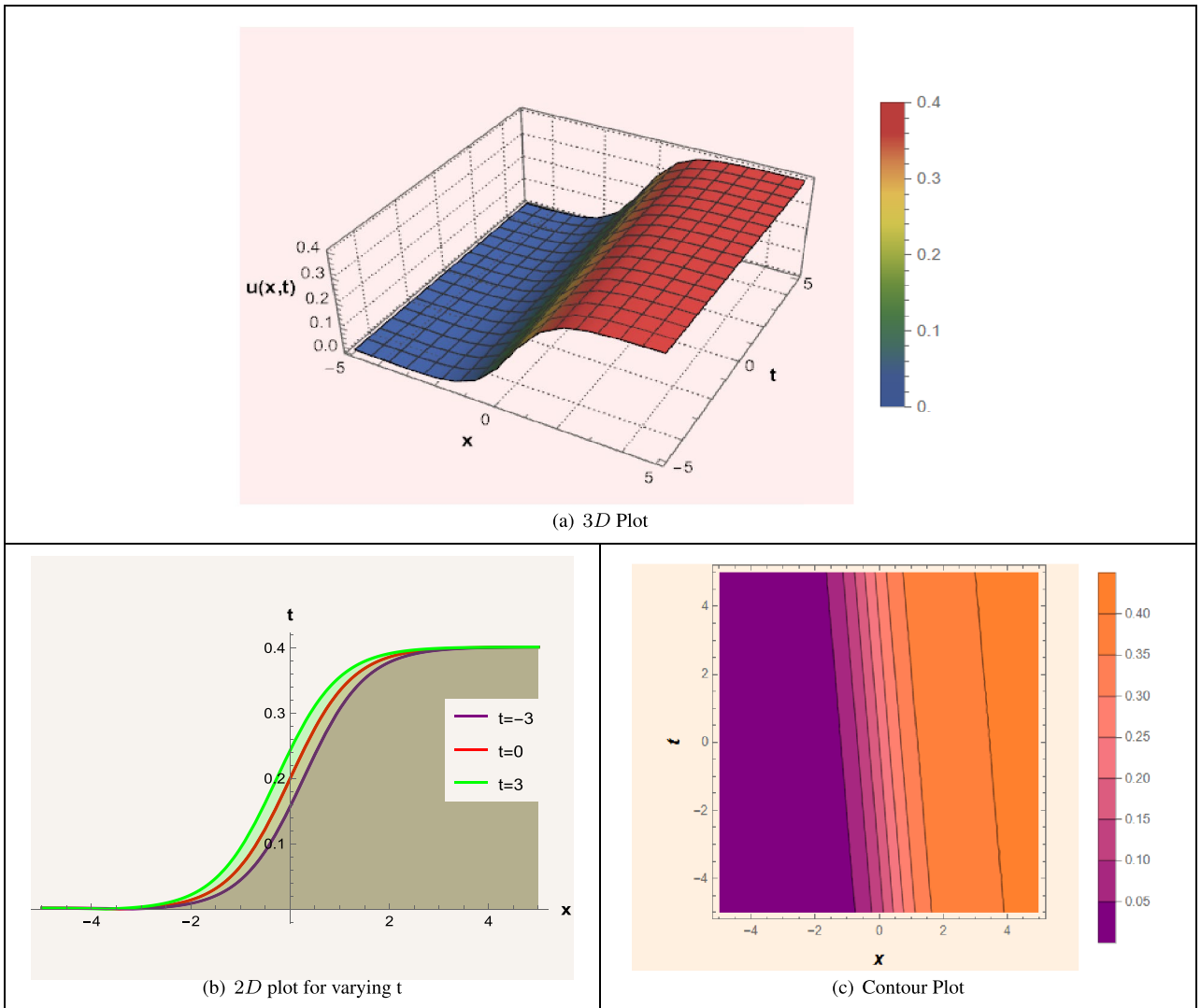


Fig. 3. Absolute behaviour for Eq. (4.6) represent anti-kink soliton obtained by employing the parametric values: (a) 3D plot illustrates the transition profile along the x-t. plane; (b) 2D profiles demonstrate the phase shift at $t = 0$ (red line), $t = -3$ (purple line) and $t = 3$ (green line); (c) Contour graph shows the kinetics of phase reversal throughout the propagation domain.

Parameters values for all solutions-type (dark, anti-kink, periodic, V-shaped and kink) is given in Table 1 for clarity. These visualizations and propagation stability provide an intuitive representation of the wave structures, phase transitions, and space distributions that are necessary for the analysis of the physical mechanism.

Bifurcation analysis

Bifurcation in dynamical systems occurs when small parameter changes result in large changes in the system's behavior. This can involve the appearance of periodic patterns, chaotic dynamics or new stable phases. The bifurcation hypothesis describes these abrupt changes and even forecasts how systems evolve through various phases of their behavior. One well-documented real-world example is the way that traffic patterns on a road change. With more cars on the road, the system can transition suddenly from free-flowing traffic to dense stop-and-go waves. This bifurcation describes how a small parameter change (e.g., in car density) results in a large change in the system's behavior^{28,29}.

Let $\frac{d\Psi}{d\xi} = N$, then the planar dynamical system of equation Eq. (4.3) is:

$$\text{Planar dynamical system : } \begin{cases} \frac{d\Psi}{d\xi} = N, \\ \frac{dN}{d\xi} = V_1\Psi - V_2\Psi^3. \end{cases} \tag{6.1}$$

With Hamiltonian function:

$$H(\Psi, N) = \frac{N^2}{2} - \frac{V_1\Psi^2}{2} + \frac{V_2\Psi^4}{4} = h,$$

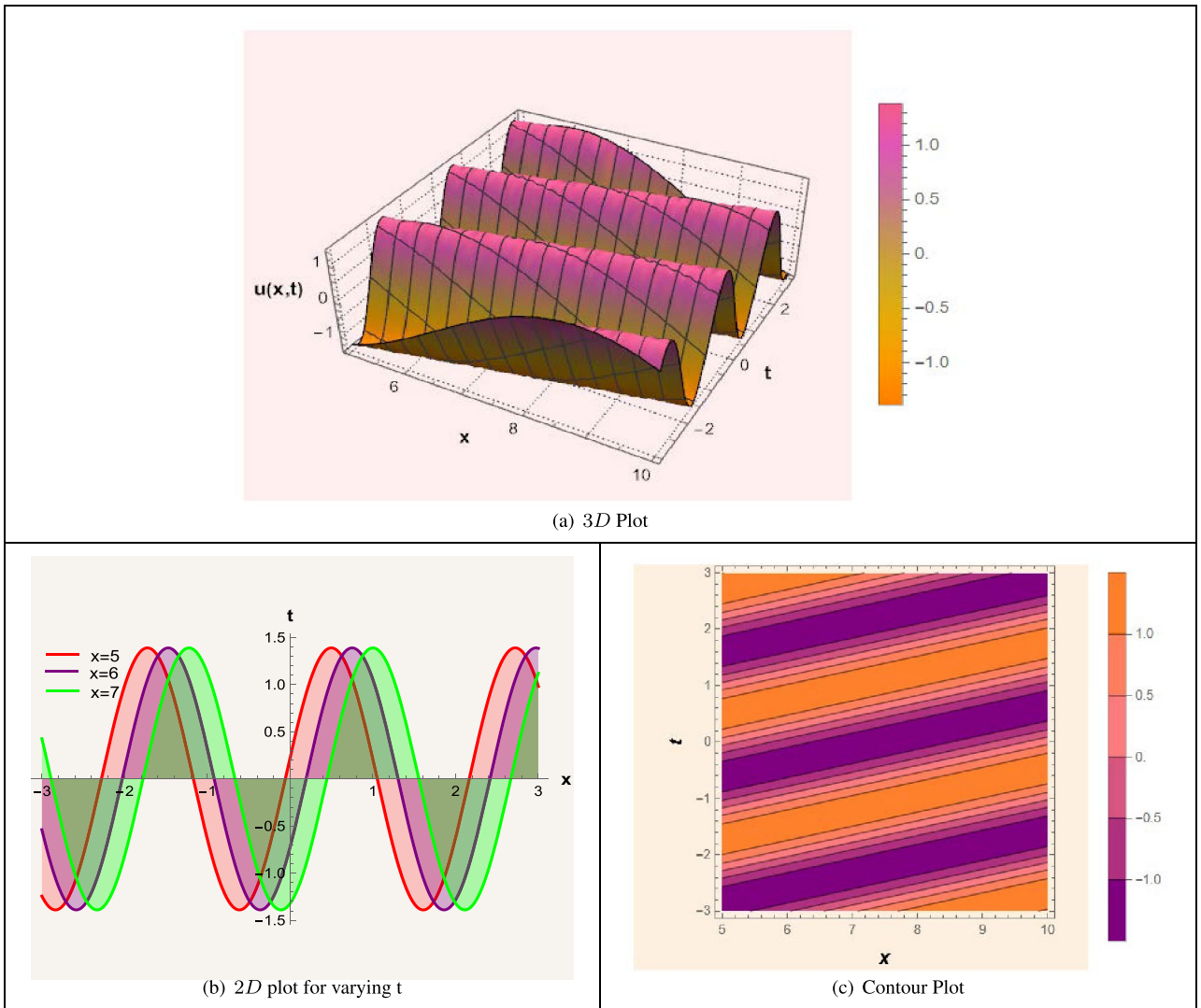


Fig. 4. Periodic wave solution of real behaviour for Eq. (4.7) with the parametric values: (a) 3D plot illustrates the periodic wave along the x-t plane; (b) 2D profiles demonstrate wave at $x = 5$ (red line), $x = 6$ (purple line) and $x = 7$ (green line); (c) Contour plot depicts phase matching within the periodic structure.

where, h is Hamiltonian constant, $V_1 = (\gamma + 3\eta^2)$ and $V_2 = \frac{\beta_2 + 2\beta_3}{3}$. It is important to note that the four parameter cases in the phase portraits are not arbitrarily selected. They arise naturally from the different sign combinations of the coefficients V_1 and V_2 in the reduced dynamical system Eq. (6.1). Each case determines whether the equilibrium points act as centers, saddles, or cuspidal points, thereby covering all qualitatively distinct dynamical behaviors of the system. Physically, these cases correspond to regimes governed by different balances between dispersion and nonlinearity. For instance, positive or negative values of V_1 and V_2 represent scenarios relevant to optical fibers, plasma waves, and fluid systems under different operating conditions. Hence, the four cases are both mathematically exhaustive and physically meaningful, providing a comprehensive view of the system's dynamics.

In hamiltonian, $\frac{1}{2}N^2$ represent kinetic energy, and $\frac{V_1\Psi^2}{2} + \frac{V_2\Psi^4}{4}$ denotes potential energy. For equilibrium points, put $\frac{d\Psi}{d\xi} = 0$, then Eq. (6.1) becomes:

$$\begin{cases} N = 0, \\ V_1\Psi - V_2\Psi^3 = 0. \end{cases} \tag{6.2}$$

Solving this system yields, $(0, 0), \left(-\frac{\sqrt{V_1}}{\sqrt{V_2}}, 0\right), \left(\frac{\sqrt{V_1}}{\sqrt{V_2}}, 0\right)$.

The determinant of the Jacobian matrix of Eq. (6.1) is

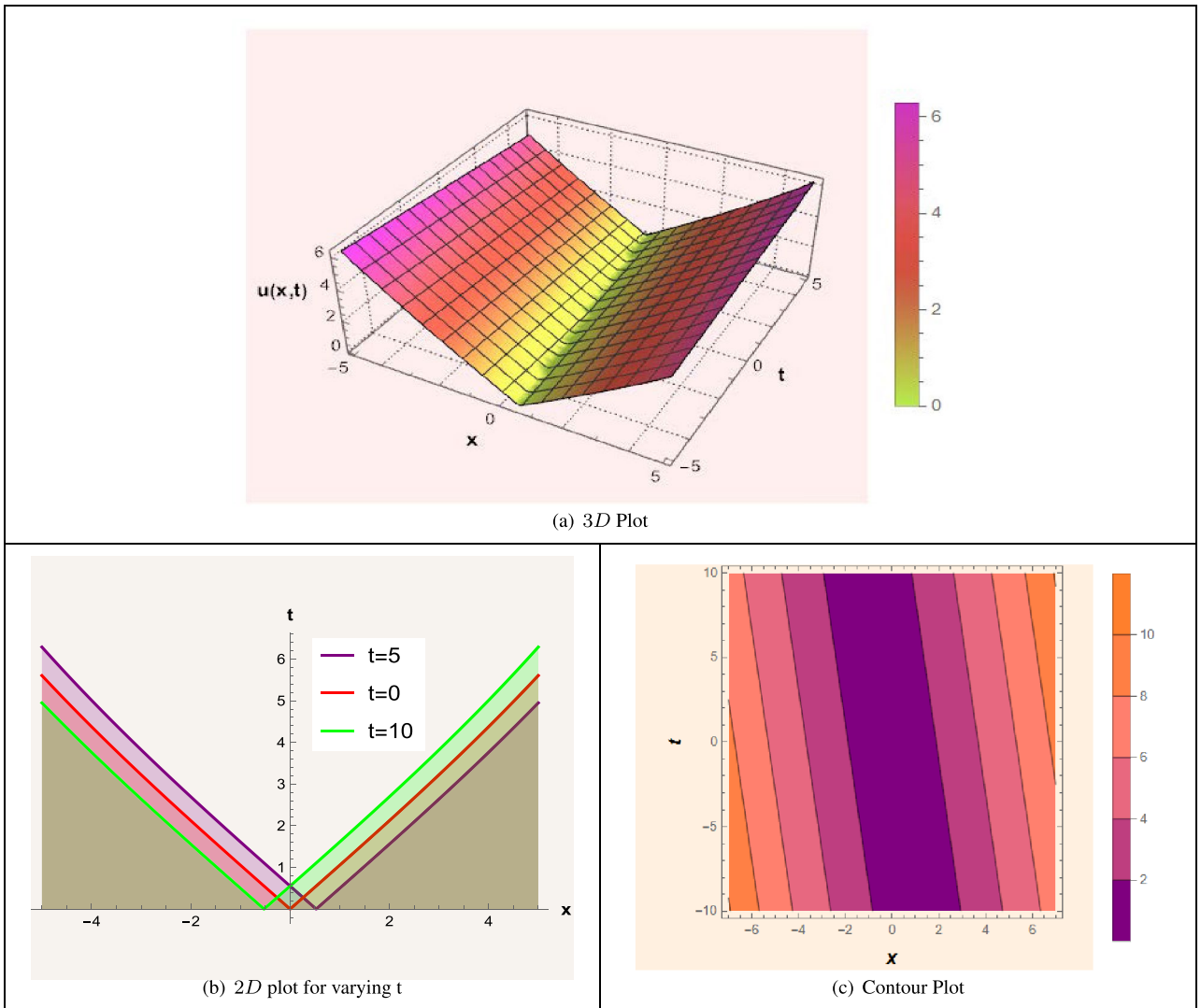


Fig. 5. V-soliton solution of absolute behaviour for Eq. (4.8) with the parametric values: (a) 3D plot illustrates the propagation of V-shaped profile along the x-t plane; (b) 2D profiles at $t = 0$ (red line), $t = -5$ (purple line) and $t = 5$ (green line); (c) Contour map depicts the combined effect of spectral broadening and phase shift dynamics.

$$J(\Psi, N) = \begin{vmatrix} 0 & 1 \\ -3V_2 \Psi^2 + V_1 & 0 \end{vmatrix} = 3V_2 \Psi^2 - V_1.$$

Consequently,

- If $J(\Psi, N) < 0$, then $(\Psi, 0)$ represent saddle point.
- If $J(\Psi, N) > 0$, then $(\Psi, 0)$ represent center point.
- If $J(\Psi, N) = 0$, then $(\Psi, 0)$ represent cuspidal point.

Changing the values of parameters results in four case:

Case 1: Figure 7a illustrates the case $V_1 > 0, V_2 > 0$ with the equilibrium points $(0, 0), (-2, 0)$ and $(2, 0)$ under the parameters $\gamma = 5, \eta = 1, \beta_2 = 4, \beta_3 = 1$, where $(0, 0)$ is saddle point and $(\pm 2, 0)$ represent center points.

Case 2: Figure 7b illustrates the case $V_1 < 0, V_2 < 0$ with equilibrium points $(0, 0), (-3, 0)$ and $(3, 0)$ under the parameters $\gamma = -12, \eta = -1, \beta_2 = -5, \beta_3 = 1$, where $(0, 0)$ denotes center point and $(\pm 3, 0)$ represent saddle points.

Case 3: Figure 7c illustrates the case $V_1 > 0, V_2 < 0$ with equilibrium points $(0, 0), (-2\iota, 0)$ and $(2\iota, 0)$ under the parameters $\gamma = 1, \eta = 1, \beta_2 = -5, \beta_3 = 1$, where $(0, 0)$ denotes saddle point and $(\pm 2\iota, 0)$ represent center-like points.

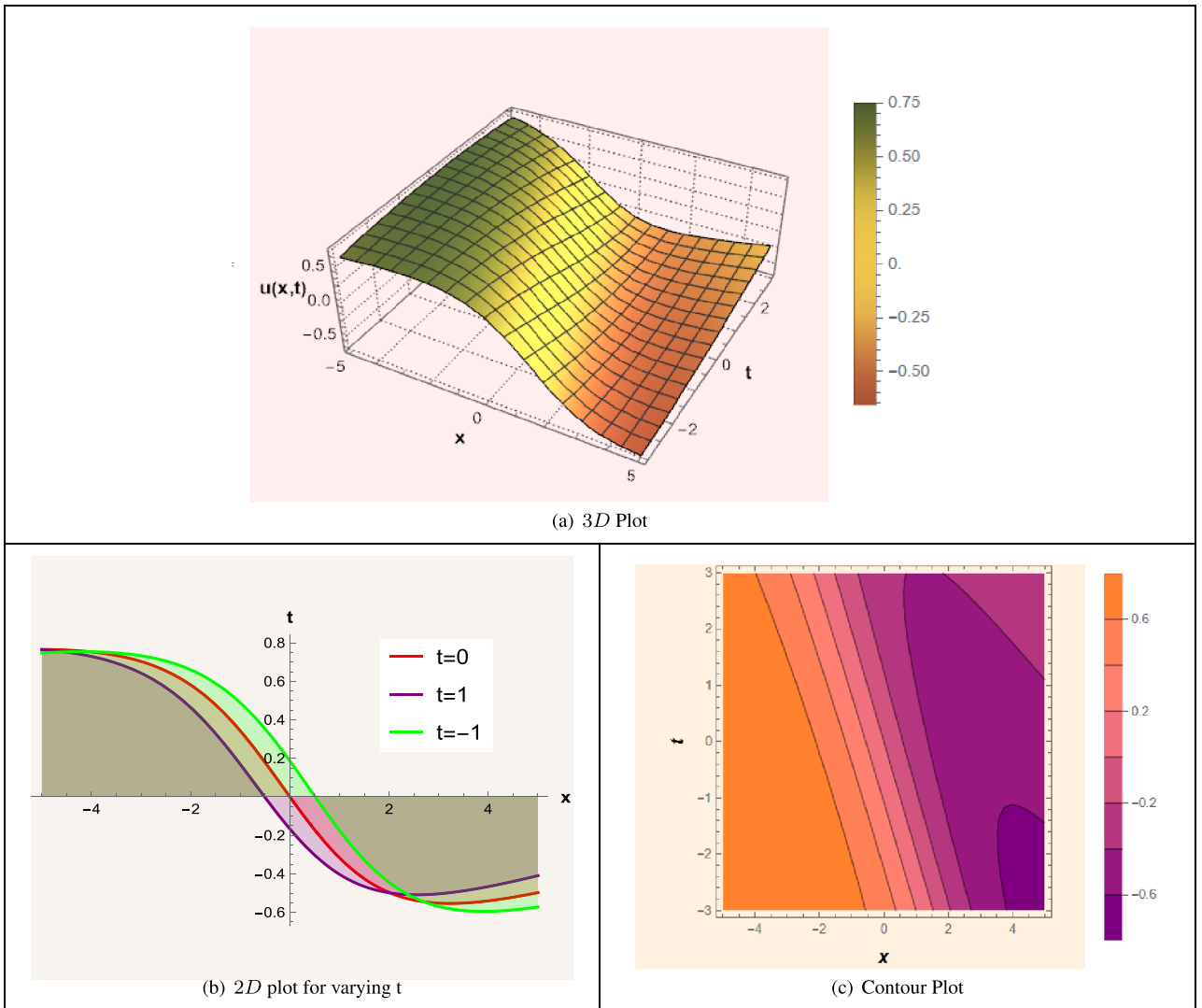


Fig. 6. Kink soliton solution of imaginary behaviour for Eq. (4.8) with the parametric values: (a) 3D plot illustrates the phase transition along the x-t plane; (b) 2D plot demonstrate phase shift at $t = 0$ (red line), $t = 1$ (purple line) and $t = -1$ (green line); (c) Contour map illustrate the phase shift dynamics.

Figures	Parameter values
Figure 2	$\delta = 1, \eta = 0.21, c_0 = -1.1, \theta = 0.5, \zeta = -0.9, \chi = 0.1$
Figure 3	$\delta = 2, \eta = 0.5, c_0 = 0.1, \theta = \zeta = -0.7, \chi = 0.8$
Figure 4	$\delta = 1, \eta = -0.71, c_0 = 0.8, \theta = \zeta = -0.9, \chi = -0.5$
Figure 5	$\delta = -0.7, \eta = -0.2, c_0 = 7, \theta = \zeta = 0.1, \chi = -0.1$
Figure 6	$\delta = 1.2, \eta = 0.1, c_0 = -0.8, \theta = \zeta = 0.1, \chi = -1$

Table 1. Summary of parameters used for different solutions.

Case 4: Figure 7d illustrates case $V_1 < 0, V_2 > 0$ with equilibrium points $(0, 0), (-\iota, 0)$ and $(\iota, 0)$ under the parameters $\gamma = -4, \eta = 1, \beta_2 = 5, \beta_3 = -1$, where $(0, 0)$ is center point and $(\pm \iota, 0)$ represent saddle points.

Chaotic behaviour

Chaotic behavior is dynamics that are seen as random or unpredictable but are really governed by hidden irregular patterns. These systems are highly sensitive to initial conditions. Chaotic systems are, however, founded

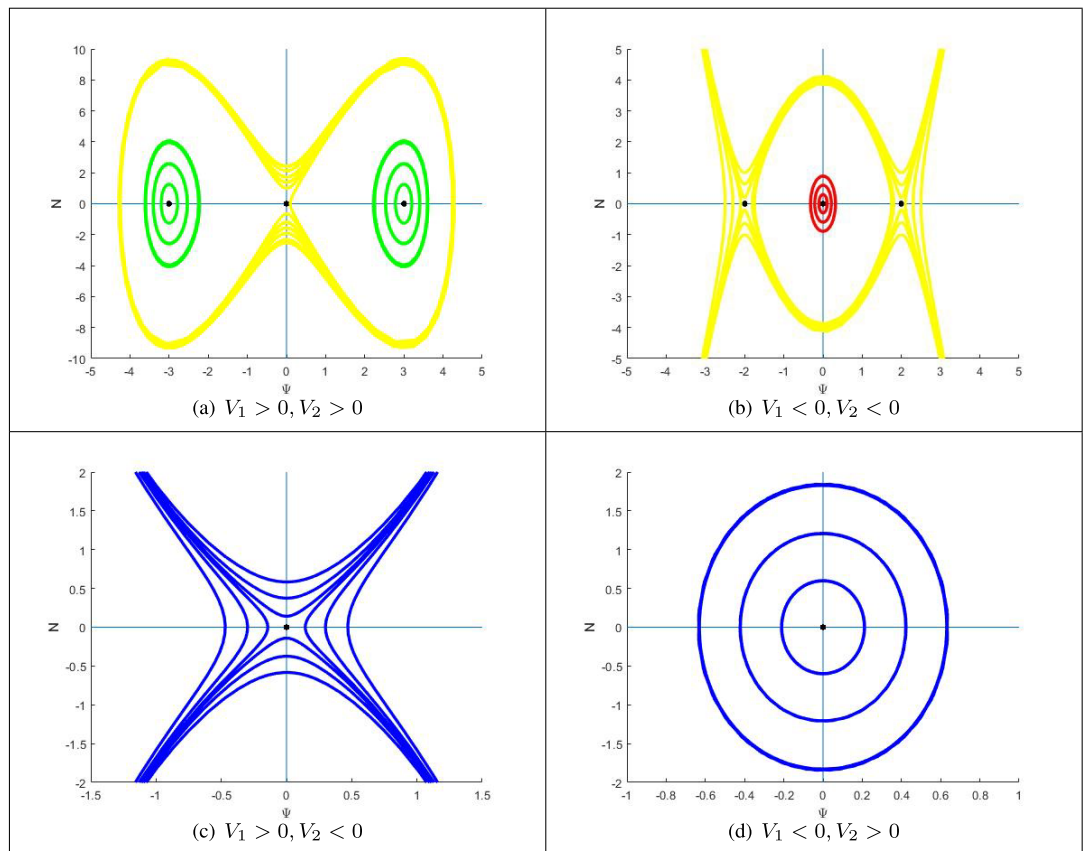


Fig. 7. Phase diagrams for planar system in Eq. (6.1): (a) illustrate the phase portrait for Case 1; (b) illustrate the phase portrait for Case 2; (c) illustrate the phase portrait for Case 3; (d) illustrate the phase portrait for Case 4.

on deterministic rules that are transparent and comprehensible through certain geometries or structures. Chaos can be observed in natural and artificial systems such as optics, atmospheric flow, and fluid dynamics.

Here, we study the chaotic behavior of the resulting dynamical system through the structures of instability. In this study, we have a careful comparison of the 2D and 3D phase portraits. To proceed with this study, we focus our attention to the second term included in Eq. (6.1).

$$\begin{cases} \frac{d\Psi}{d\xi} = N, \\ \frac{dN}{d\xi} = V_1\Psi - V_2\Psi^3 + \zeta \cos(\rho\xi). \end{cases} \quad (7.1)$$

where, ζ and ρ represents the frequency distribution and external disturbance, respectively.

Now, consider the parameter values $\gamma = 5$, $\eta = 1$, $\beta_2 = 4$, $\beta_3 = 1$. We examine how the system is affected by frequency ζ and perturbation ρ . Figures 8, 9 and 10 show chaotic behaviour of the system (6.1) for different values of ρ and ζ . The detailed description of these figures are described in the captions. These findings verify the existence of chaotic behavior in the system with the provided parameters. Generally, these graphs demonstrate the system to be chaotic, with sensitive dependence on initial values and no steady or recurring action.

To provide a quantitative verification of chaos in addition to qualitative phase portraits and time series, we computed the largest Lyapunov exponent (LLE) of the reduced planar dynamical system using the standard Benettin–Wolf algorithm with RK4 integration. The parameters were selected according to the chaotic regimes presented in Section 7. Specifically, for $V_1 = 8$ and $V_2 = 2$ corresponding to $\gamma = 5$, $\eta = 1$, $\beta_2 = 4$ and $\beta_3 = 1$, the LLE values were found to be positive across the tested cases: $\lambda_{max} \approx 0.041$ for $\zeta = 0.1$ and $\rho = 2$; $\lambda_{max} \approx 0.067$ for $\zeta = 3$ and $\rho = 2\pi$; and $\lambda_{max} \approx 0.052$ for $\zeta = 3$ and $\rho = 10$. The positivity of these exponents confirms the presence of sensitive dependence on initial conditions, thereby offering strong numerical evidence of chaotic dynamics in the GTNSE system.

Sensitivity analysis

The sensitivity analysis is carried out to examine the reaction of the dynamical system to small variations in its initial conditions. Precisely, when small changes in initial values bring about slight differences in the evolution of the system, it is classified as low sensitivity. However, when small initial perturbations cause substantial variations in system behavior, it indicates high sensitivity. In this analysis, various solution curves are seen for constant

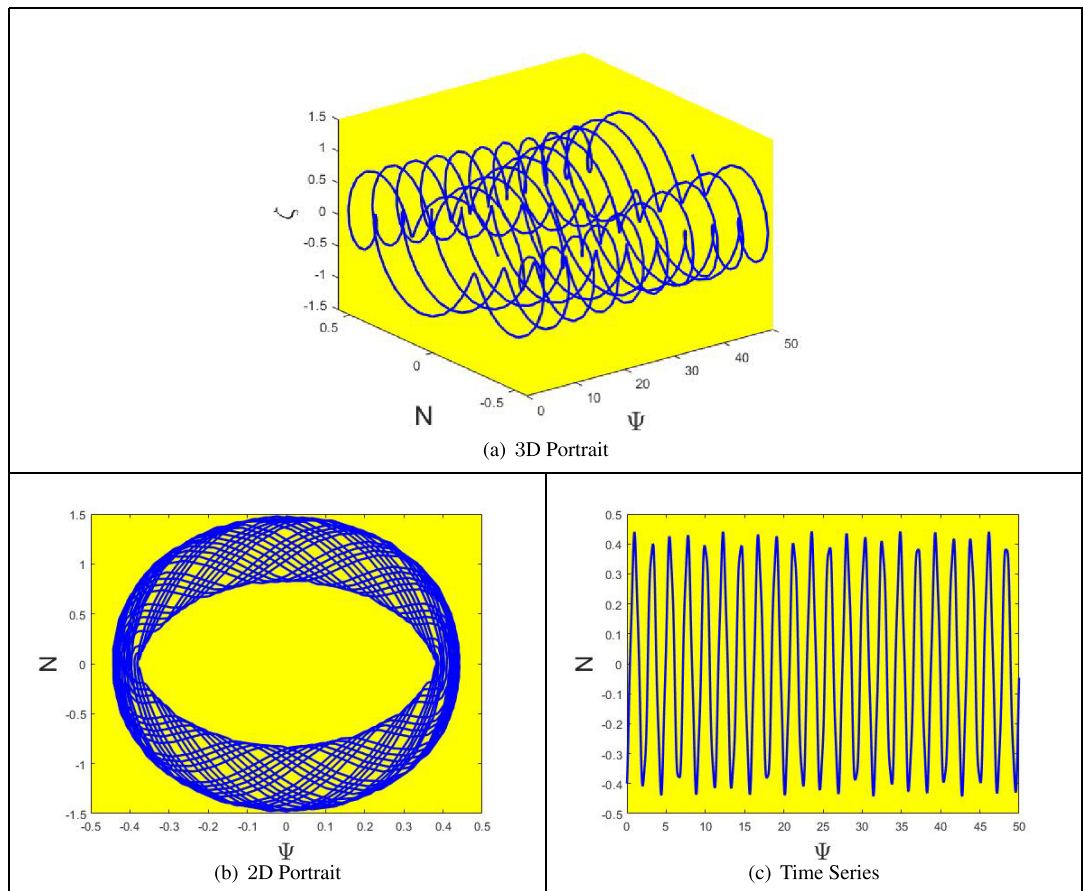


Fig. 8. Chaotic nature of the system (6.1) for $\rho = 2$ and $\zeta = 0.1$.

parameters: $\gamma = 5$, $\eta = 1$, $\beta_2 = 4$, $\beta_3 = 1$, to analyze how the stability changes of Eq. (6.1), when the initial conditions are slightly modified. In Fig. 11, two solution paths are plotted $(\Psi(0), N(0)) = (0.7, 0.2)$ with red and $(\Psi(0), N(0)) = (0.7, 1.5)$ with blue line. In Fig. 12, two orbits are shown again: $(\Psi(0), N(0)) = (0.7, 0.1)$ in red and $(\Psi(0), N(0)) = (0.9, 0.3)$ in green. In Fig. 13, two additional initial condition pairs are used: $(\Psi(0), N(0)) = (0.9, 0.9)$ in green and $(\Psi(0), N(0)) = (0.6, 0.3)$ in blue. In Fig. 14, three initial conditions are tested: $(\Psi(0), N(0)) = (0.7, 0.8)$ in red and $(\Psi(0), N(0)) = (0.5, 0.3)$ in green. Graphical inspection shows that even slight variations in $(\Psi(0), N(0))$ result in visible alterations in solution behavior, demonstrating the system's strong sensitivity to initial conditions. This is a significant observation in confirming the responsiveness and rich dynamics of the model, which can lead to unstable behaviors under a small change in inputs.

In addition to graphical inspection, the sensitivity of the system can also be interpreted in a quantitative sense. Small perturbations in initial conditions lead to trajectories that diverge at an exponential rate, which is consistent with a positive largest Lyapunov exponent. This implies that the growth rate of separation between initially close trajectories serves as a measurable indicator of sensitivity. Hence, while our visual results illustrate the phenomenon effectively, they are also supported by the underlying dynamical system theory that confirms sensitivity through norms and growth rates.

It is worth noting that the sensitivity outcomes are directly aligned with the stability conditions established in the bifurcation analysis. In particular, the bounded and regular trajectories observed under small perturbations correspond to the center-type equilibria, confirming local stability. Conversely, the unbounded divergence of nearby trajectories reflects the presence of saddle-type equilibria, which denote instability. This consistency between bifurcation-based classification and sensitivity responses provides a robust validation of the dynamical behavior of the system and emphasizes how small perturbations may trigger transitions predicted by the bifurcation framework.

Physical interpretation

The GTNSE plays a central role in the description of nonlinear wave propagation in a variety of physical systems. The mathematical formulation includes higher-order dispersion, self-phase modulation, self-steepening phenomena, and nonlocal nonlinear interactions. Its implications are present in fields including nonlinear optics, fluid dynamics, plasma physics, and Bose-Einstein condensates, where the interplay between dispersion and nonlinearity is the controlling influence on the subtle dynamics of wave propagation. The applications of terms involving in equation are describe below:

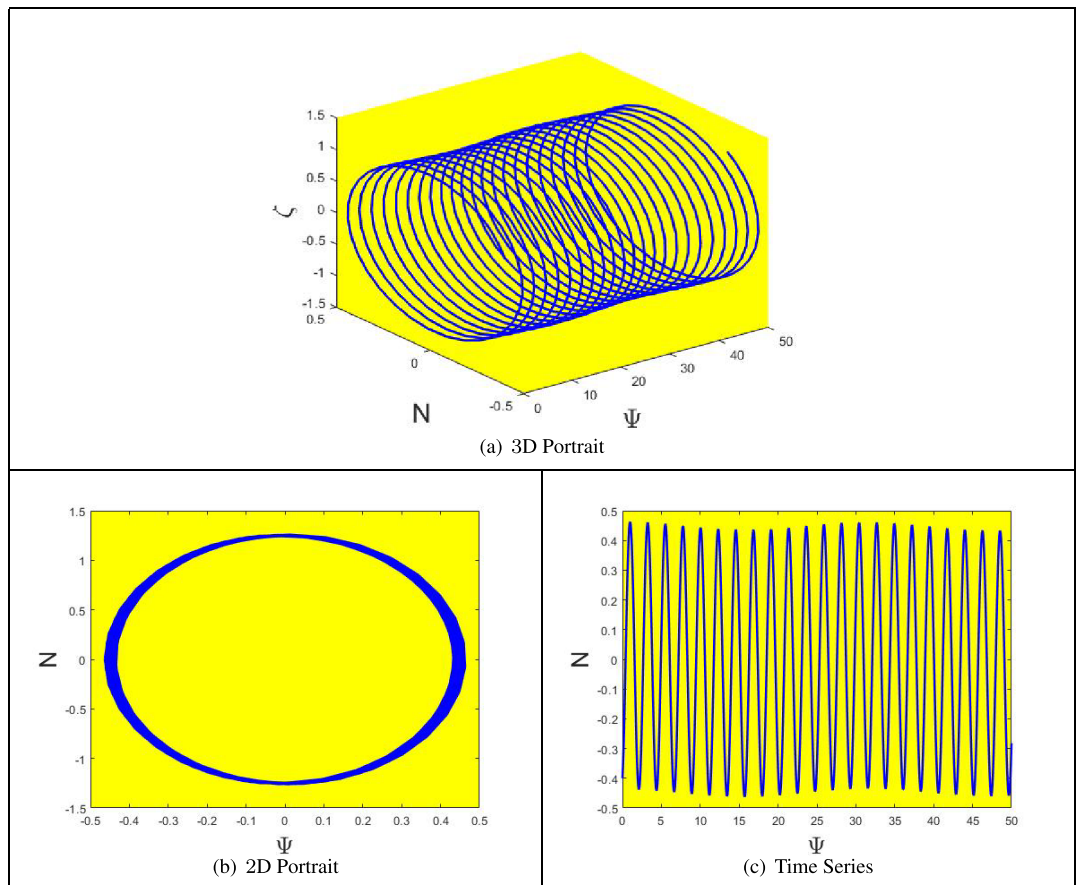


Fig. 9. Chaotic nature of the system (6.1) for $\zeta = 3$ and $\rho = 2\pi$.

- Temporal evolution term ιu_t is a measure of how the wave envelope $u(x, t)$ varies with time, which describes how the shape of the wave evolves with time. Application Seen in optical fiber communication systems, in plasma waves, and in the investigation of how water waves evolve with time
- Third-order dispersion term ιu_{xxx} refers to higher-order dispersion effects, which illustrate how various frequency components of the wave travel at various velocities. Extremely important for propagation of ultrashort pulses in optical fibers, creation of supercontinuum, and study of internal ocean waves where third-order dispersion is important.
- Cubic nonlinearity (Kerr effect $\beta_1 u |u|^2$) illustrates how self-phase modulation occurs due to the Kerr effect. The refractive index varies as intensity varies, causing phase shifts and contributing to the formation of solitons. Application finds in optical fiber communications (soliton pulses), Bose-Einstein condensates, water wave packets.
- The term $i\beta_2 u_x |u|^2$ explains the self-steepening phenomenon, in which areas of high-intensity waves phase shift faster, leading to pulse distortion and steepening. The phenomenon is important for short, high-intensity pulses in nonlinear fiber optics and is significant for supercontinuum light sources.
- $\iota \beta_3 (|u|^2)_x u$ defines excited Raman scattering or higher order nonlinear dispersion. Enables energy transfer between higher and lower frequencies (self-frequency shift), typically manifesting itself as the Raman effect or nonlinear spectral recoil. The phenomenon is important in fiber optics (soliton self-frequency shift, Raman scattering), acoustic phonon coupling, energy transfer in plasmas.

The NAEM is an analytical tool for obtaining exact solutions to nonlinear evolution equations, which are essential in mathematics, physics, and engineering. The method is effective in producing many different exact solutions—kink, anti-kink, periodic, V-type, and dark soliton solutions—characterizing real-world wave phenomena. Kink and anti-kink soliton solutions are characterized by sudden jumps between two states. This renders them suitable for the description of magnetic domain walls, nerve impulses in biological systems, and phase boundaries in condensed matter physics. In nonlinear optics, for instance, a kink soliton can possess the sudden leading edge of an optical pulse when it makes a jump between two states of intensity. This is significant in signal processing and optical switching devices. Periodic solutions have recurring wave patterns. They are useful in naturally repeating systems, like the propagation of energy in crystal structures, sound waves in periodic media, and water wave dynamics. Periodic solutions are especially important in the case of repeating boundary optical fibers and in photonic crystals, where wave propagation is governed by periodicity in the refractive index. Temporal

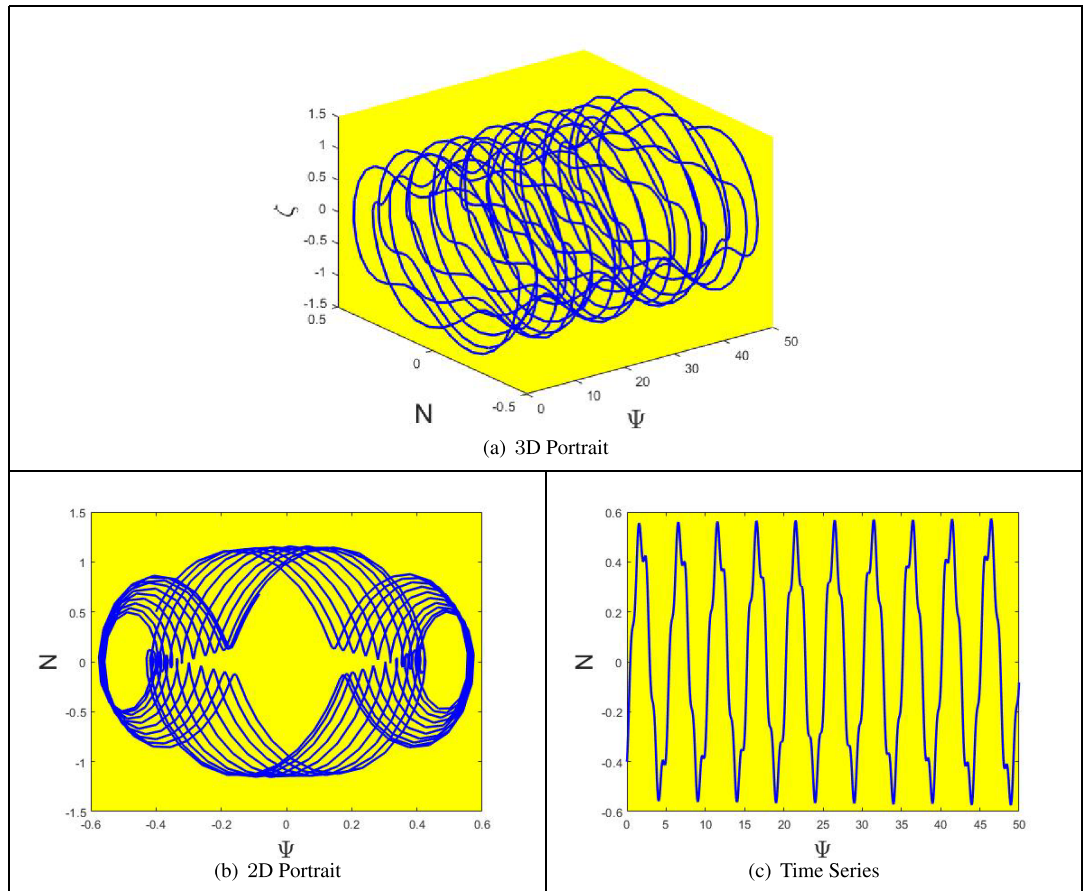


Fig. 10. Chaotic behaviour of the system (6.1) for $\zeta = 3$ and $\rho = 10$.

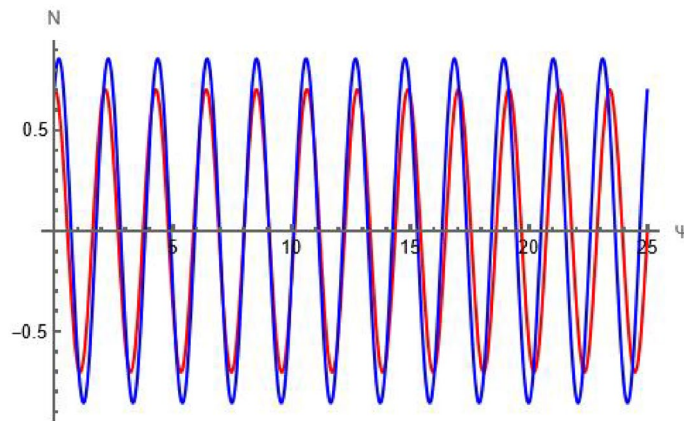


Fig. 11. Sensitivity response by considering two conditions: $(\Psi(0), N(0)) = (0.7, 0.2)$ and $(\Psi(0), N(0)) = (0.7, 1.5)$, which are represented by lines in red and blue, respectively.

dark solitons have been experimentally demonstrated in optical fibers, where dark solitons propagate as "holes" on a continuous-wave background. One experiment used $5.3ps$ dark solitons generated from $36ps$ wide pulses generated from an $850nm$ titanium-doped sapphire laser, and then propagating $1km$ of optical fiber. This is used in nonlinear guided wave optics and optical switching. Kink solitons have been utilized as useful applications in the form of polarization switches and optical logic gates in nonlinear optics. They are employed in modeling

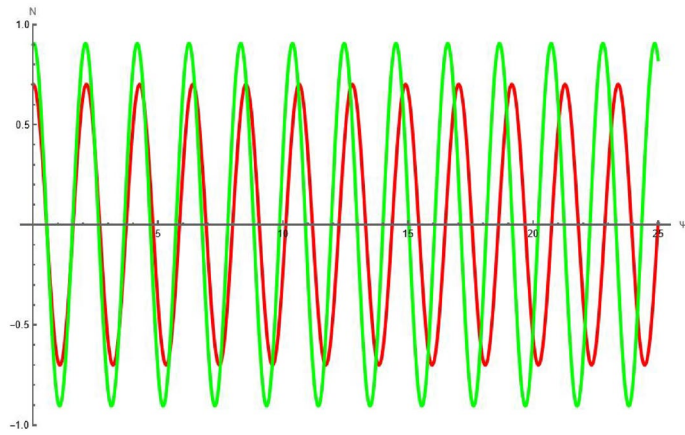


Fig. 12. Sensitivity response by considering two conditions: $(\Psi(0), N(0)) = (0.7, 0.1)$ and $(\Psi(0), N(0)) = (0.9, 0.3)$, which are represented by lines in red and green, respectively.

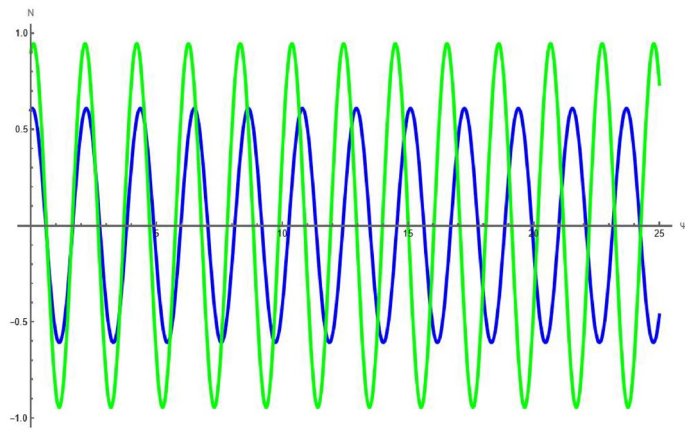


Fig. 13. Sensitivity response by considering two conditions: $(\Psi(0), N(0)) = (0.9, 0.9)$ and $(\Psi(0), N(0)) = (0.6, 0.3)$, which are represented by lines in green and blue, respectively.

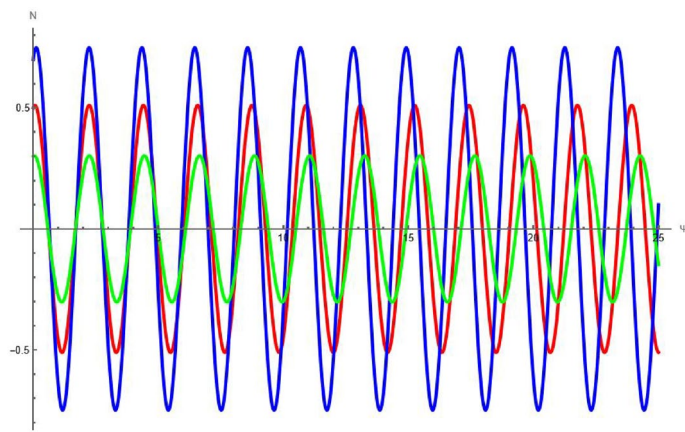


Fig. 14. Sensitivity profile under conditions: $(0.5, 0.3)$, $(0.3, 0.1)$ and $(0.7, 0.8)$ represented by blue, green and red, respectively.

dislocation dispersion in crystals and wave propagation in plasmas. Their stability and topological nature have been investigated through experimental and theoretical studies, and in applications in fluid dynamics and quantum field theory. Anti-kink solitons, which are often studied alongside kink solitons in specific systems, especially Sine-Gordon-type systems, are topological solitons like particle-antiparticle wave objects in condensate matter and nonlinear wave systems. Experimental and theoretical work has studied their dynamic interactions (kink-antikink collisions). V-shaped dark solitons were investigated in relation to their propagation characteristics in inhomogeneous optical fibers, their behavior and shape being controllable to enable soliton control in optical communication systems. Periodic wave train or periodic soliton solutions have been generated in birefringent fibers for pulse shaping and nonlinear fiber optics. Experimental demonstration shows varied envelope soliton pulses periodic or multi-peak structures such as W-shaped solitons. It is important to note that the physical relevance of the obtained solutions is strongly dependent on parameter selection. Our bifurcation and sensitivity analyses demonstrate that while stable soliton, periodic, and kink-type structures exist in specific regimes, certain parameter combinations lead to instability or chaotic behavior. In these cases, the Hamiltonian structure of the unperturbed system may be destroyed, resulting in non-conservation of energy and loss of physical applicability. Thus, the derived analytical solutions remain valid in form, but their stability and physical significance are restricted to ranges where the balance between dispersion and nonlinearity is preserved.

Conclusion

This paper investigates the GTNSE comprehensively by a new powerful method known as the auxiliary equation method. The proposed method is found to be very efficient for analytically solving considered equation when compared with classical methods of solutions. In contrast to classical procedures that can have difficulty with the intricate higher-order terms and complicated nonlinear interactions involved in the considered equation, NAEM method systematically reduces the PDE into a more tractable ODE through wave transformations and simplifications. This makes possible the derivation of exact solutions, including V-shaped, kink, dark soliton, periodic, and anti-kink solitons, without losing the key nonlinear and dispersive features of the system. Each of them is obtained and explained carefully mathematically. These solutions significantly enrich the known type of solutions for this significant class of nonlinear wave equations, demonstrating how efficient the method is in handling complicated nonlinear evolution equations. The dynamical behaviors of the system were explored in depth with the help of an advanced analytical Galilean transformation. Hamiltonian formalism provided valuable information about the conserved quantities and stability properties of the system, and phase portrait construction revealed the rich dynamics at play, such as periodic, quasi-periodic, and chaotic phases. Bifurcation analysis charted the significant points of transition between solution types and provided valuable information on parameter dependence and solution stability. To gain further insight, we conducted a careful sensitivity analysis to see how the system responds to changes in parameters and initial conditions. This was found to reveal strong solution patterns and to indicate when chaotic behavior can arise. The mathematical formalism reached here presents new avenues of research, including its extension to higher-dimensional systems, investigation of coupled nonlinear systems, and investigation of other solution classes using higher-level tools. Physically, the findings provide insight into nonlinear wave propagation in optical fibers, plasma, and fluid systems where higher-order effects like dispersion, self-steepening, and Raman scattering are important. Not only does this work enlarge the solution space of proposed equation but also sets a strong platform for applications in photonics, high-speed communications, and other nonlinear physical systems. The results here not only provide a basis for improving our simple conceptual image of nonlinear wave equations but also give a solid theoretical foundation for the investigation of similar systems in mathematical physics. Future prospects include the extension of these methods to other physically interesting nonlinear evolution equations and investigation of potential applications in other fields of physics and engineering.

Data availability

The data and materials used to support the findings of this study are included in this article.

Received: 23 July 2025; Accepted: 10 September 2025

Published online: 14 October 2025

References

1. Helal, M. A. & Seadawy, A. R. Benjamin-Feir instability in nonlinear dispersive waves. *Comput. Math. Appl.* **64**(11), 3557–3568 (2012).
2. Zabusky, N. J. & Kruskal, M. D. Interaction of solitons in a collisionless plasma and the recurrence of initial states. *Phys. Rev. Lett.* **15**(6), 240 (1965).
3. Lu, D., Seadawy, A. R., Wang, J., Arshad, M. & Farooq, U. Soliton solutions of the generalised third-order nonlinear Schrödinger equation by two mathematical methods and their stability. *Pramana* **93**(3), 44 (2019).
4. Behera, S. Analysis of traveling wave solutions of two space-time nonlinear fractional differential equations by the first-integral method. *Mod. Phys. Lett. B* **38**(04), 2350247 (2024).
5. Behera, S. & Aljahdaly, N. H. Soliton solutions of nonlinear geophysical KdV equation via two analytical methods. *Int. J. Theor. Phys.* **63**(5), 107 (2024).
6. Behera, S. Optical solitons for the Hirota–Ramani equation via improved $(\frac{G'}{G})$ -expansion method. *Mod. Phys. Lett. B* **39**(01), 2450403 (2025).

7. Behera, S. Multiple soliton solutions of some conformable fractional nonlinear models using Sine-Cosine method. *Opt. Quantum Electron.* **56**(7), 1235 (2024).
8. Behera, S. Computational and numerical analysis of the soliton solutions to the geophysical KdV equation using two robust analytical methods. *Pramana* **99**(3), 108 (2025).
9. Alquran, M. Investigating fluctuation varieties in the propagation of the perturbed KdV equation with time-dependent perturbation coefficient. *Partial Differ. Equ. Appl. Math. matics* **14**, 101206 (2025).
10. Alquran, M. & Alhami, R. Analysis of lumps, single-stripe, breather-wave, and two-wave solutions to the generalized perturbed-KdV equation by means of Hirota's bilinear method. *Nonlinear Dyn.* **109**(3), 1985–1992 (2022).
11. Alquran, M. Physical properties for bidirectional wave solutions to a generalized fifth-order equation with third-order time-dispersion term. *Results Phys.* **28**, 104577 (2021).
12. Alquran, M. Variation of the influence of Atangana-conformable time-derivative on various physical structures in the fractional KP-BBM model. *Int. J. Theor. Phys.* **63**(9), 225 (2024).
13. Alquran, M. Necessary conditions for convex-periodic, elliptic-periodic, inclined-periodic, and rogue wave-solutions to exist for the multi-dispersions Schrödinger equation. *Phys. Scr.* **99**(2), 025248 (2024).
14. Alquran, M. & Al-deiakeh, R. Lie-Backlund symmetry generators and a variety of novel periodic-soliton solutions to the complex-mode of modified Korteweg-de Vries equation. *Qual. Theory Dyn. Syst.* **23**(2), 95 (2024).
15. Jaradat, I., Alquran, M., Ali, M. & Al-deiakeh, R. Modeling synchronized propagation of two symmetric waves in a new two-mode extension of the $(1 + 1)$ -dimensional Chaffee-Infante model. *Int. J. Theor. Phys.* **64**(2), 45 (2025).
16. Alquran, M. New interesting optical solutions to the quadratic-cubic Schrodinger equation by using the Kudryashov-expansion method and the updated rational sine-cosine functions. *Opt. Quantum Electron.* **54**(10), 666 (2022).
17. Pan, J., Rahman, M. U. & Rafiullah, U. Breather-like, singular, periodic, interaction of singular and periodic solitons, and a-periodic solitons of third-order nonlinear Schrödinger equation with an efficient algorithm. *Eur. Phys. J. Plus* **138**(10), 912 (2023).
18. Nasreen, N., Seadawy, A. R., Lu, D. & Arshad, M. Optical fibers to model pulses of ultrashort via generalized third-order nonlinear Schrödinger equation by using extended and modified rational expansion method. *J. Nonlinear Opt. Phys. Mater.* **33**(04), 2350058 (2024).
19. Ahmed, A. I. et al. Dynamical behavior of the fractional generalized nonlinear Schrödinger equation of third-order. *Opt. Quantum Electron.* **56**(5), 843 (2024).
20. Badshah, F., Tariq, K. U., Inc, M. & Kazmi, S. R. Solitons, stability analysis and modulation instability for the third order generalized nonlinear Schrödinger model in ultraspeed fibers. *Opt. Quantum Electron.* **55**(12), 1094 (2023).
21. Faridi, W. A. et al. Analyzing optical soliton solutions in Kairat-X equation via new auxiliary equation method. *Opt. Quantum Electron.* **56**(8), 1317 (2024).
22. Kazmi, S. S. et al. The analysis of bifurcation, quasi-periodic and solitons patterns to the new form of the generalized q-deformed Sinh-Gordon equation. *Symmetry* **15**(7), 1324 (2023).
23. Behera, S., Mohanty, S. & Virdi, J. P. S. Analytical solutions and mathematical simulation of traveling wave solutions to fractional order nonlinear equations. *Partial Differ. Equ. Appl. Math.* **8**, 100535 (2023).
24. Behera, S. Dynamical solutions and quadratic resonance of nonlinear perturbed Schrödinger equation. *Front. Appl. Math. Stat.* **8**, 1086766 (2023).
25. Behera, S. & Aljahdaly, N. H. Nonlinear evolution equations and their traveling wave solutions in fluid media by modified analytical method. *Pramana* **97**(3), 130 (2023).
26. Seadawy, A. R., Arshad, M. & Lu, D. The weakly nonlinear wave propagation of the generalized third-order nonlinear Schrödinger equation and its applications. *Waves Random Complex Media* **32**(2), 819–831 (2022).
27. Malik, S., Kumar, S., Nisar, K. S. & Saleel, C. A. Different analytical approaches for finding novel optical solitons with generalized third-order nonlinear Schrödinger equation. *Results Phys.* **29**, 104755 (2021).
28. Li, Z., Lyu, J. & Hussain, E. Bifurcation, chaotic behaviors and solitary wave solutions for the fractional Twin-Core couplers with Kerr law non-linearity. *Sci. Rep.* **14**(1), 22616 (2024).
29. Li, Z. & Zhao, S. Bifurcation, chaotic behavior and solitary wave solutions for the Akbota equation. *AIMS Math.* **9**(8), 22590–22601 (2024).

Acknowledgements

The authors would like to acknowledge the Deanship of Graduate Studies and Scientific Research, Taif University for funding this work.

Author contributions

Mehreen Fatima: methodology, investigation, writing—original draft. Muhammad Abbas: methodology, supervision, writing—original draft, writing—review & editing. Yagoub.A.S.Arko: visualization, formal analysis, investigation, writing—review & editing. Tahir Nazir: supervision, writing—original draft, writing—review & editing. Asnake Birhanu: formal analysis, investigation, writing—review & editing. Muhammad Zain Yousaf: formal analysis, investigation, writing—review & editing. All authors have read and agreed to the published version of the manuscript.

Funding

The author(s) received no external funding for this study.

Declarations

Competing interests

The authors declare no competing interests.

Additional information

Correspondence and requests for materials should be addressed to M.A. or A.B.

Reprints and permissions information is available at www.nature.com/reprints.

Publisher's note Springer Nature remains neutral with regard to jurisdictional claims in published maps and institutional affiliations.

Open Access This article is licensed under a Creative Commons Attribution-NonCommercial-NoDerivatives 4.0 International License, which permits any non-commercial use, sharing, distribution and reproduction in any medium or format, as long as you give appropriate credit to the original author(s) and the source, provide a link to the Creative Commons licence, and indicate if you modified the licensed material. You do not have permission under this licence to share adapted material derived from this article or parts of it. The images or other third party material in this article are included in the article's Creative Commons licence, unless indicated otherwise in a credit line to the material. If material is not included in the article's Creative Commons licence and your intended use is not permitted by statutory regulation or exceeds the permitted use, you will need to obtain permission directly from the copyright holder. To view a copy of this licence, visit <http://creativecommons.org/licenses/by-nc-nd/4.0/>.

© The Author(s) 2025